Chapter 6

Simulated Quadrant Photodiode

6.1 Overview

In this chapter, we begin with a brief discussion of the working principle behind a position detection device. We then provide a framework for replicating the scattering signal recorded by a quadrant photo diode. We show that extending the framework to capture information from an arbitrary shaped particle is simple in principle but difficult to interpret, we demonstrate as such by comparing the expected signal from a trapped sphere, to that of a trapped dimer.

6.2 Introduction

Beyond merely simulating the forces experienced by a spherical aggregate we also developed a simulative quadrant photo diode to replicate the results from a typical calibration test. This builds upon the work from [4] which applied Lorenz-Mie theory to replicate the response signal of a QPD being used in back focal-plane interferometry. Rather than be constrained to individual spheres we can now consider the expected response from any type of spherical aggregate. The goal of such simulation software would be to simulate the expected experimental results from a complex particle whose exact shape and size may be difficult to determine.

In order to simulate a typical experimental set up with a QPD installed as a position

detection system we need to evaluate the total magnitude of the electric field incident on the photo-diode surface. While trapping a micro-particle, the scattered and incident fields combine together and interfere with one another. These fields are collected by a condenser lens in the far field limit and are focused onto the QPD surface, the total intensity can be evaluated as:

$$I(x,y) = \epsilon_0 c \left| \begin{bmatrix} E_{i,x}(x,y) + E_{s,x}(x,y) \\ E_{i,y}(x,y) + E_{s,y}(x,y) \\ E_{i,z}(x,y) + E_{s,z}(x,y) \end{bmatrix} \right|^2 \times step(\theta_{NA} - \theta(x,y)) \tag{6.1}$$

The last term is simply a representative step term that defines the outer limit by which we evaluate the electric field, this is analogous to our condenser lens removing noise from other light sources by only accepting light at a specific acceptance angle defined by its numerical aperture NA_c. Depending on the relative size of our particle we can adjust the acceptance angle, this has very little effect on the transverse signals, but for axial evaluations of a trapped particle the numerical aperture should be tuned so that the resultant response curve has negative slope in order to allow for axial position detection, the method for finding this angle θ_Θ is discussed in [2].

The incident beam is simple enough to define given our set up parameters, for the sake of simplicity we assume that our beam is a Laguerre-Gaussian beam of mode $[0.0, 0.0]$ (which is simply a pure Gaussian beam). *Ott* uses a point matching approach to approximate the beam shape coefficients of the incident field by fitting it to the far field estimate. From the QPD's perspective it is receiving light both from the incident and scattered beam simultaneously, as such both fields must be expressed using outgoing vector spherical harmonics.

$$E_{\text{inc}}(r) = E_0 \sum_{n}^{\infty} \sum_{m=-n}^{n} \left[a_{mn} \mathbf{M}^{(2)}_{nm}(\mathbf{r}) + b_{nm} \mathbf{N}^{(2)}_{nm}(\mathbf{r}) \right] \tag{6.2}$$

$$E_{\text{scat}}(r) = E_0 \sum_{n}^{\infty} \sum_{m=-n}^{n} \left[p_{nm} \mathbf{N}^{(2)}_{nm}(\mathbf{r}) + q_{nm} \mathbf{M}^{(2)}_{nm}(\mathbf{r}) \right] \tag{6.3}$$

Where the superscript (2) denotes an outgoing spherical harmonic function. In

order to compute the scattering from the target particle *ott* uses the T-matrix method, this is not essential for a simple sphere but is essential for complex shaped particles such as dimers. The scattered and incident fields are then combined together in the far field to get $I(x, y)$, the quadrant and overall signals are calculated via:

$$Q_i = \sum_{n,m} I(x_{i,n}, y_{i,m}) \tag{6.4}$$

$$S_x = \frac{(Q_1 + Q_2) - (Q_3 + Q_4)}{\sum I_0(x, y)} \tag{6.5}$$

$$S_y = \frac{(Q_1 + Q_3) - (Q_2 + Q_4)}{\sum I_0(x, y)} \tag{6.6}$$

$$S_z = \frac{(Q_1 + Q_2 + Q_3 + Q_4}{\sum I_0(x, y)} \tag{6.7}$$

Where the denominator is the total intensity on the QPD while there is no particle within the trap. You would expect that S_x and S_y are near identical for equal particle displacements, however due to the polarisation of the beam there will be a slight bias to the signals for motion along the direction of the polarisation vector. This is generally not an issue if the particle trajectory is sampled for a long enough time period. By converting from signal units to length units (see (**??**)) the trap shape can be discerned from the QPD signals, assuming the fluid properties are known to a high degree of accuracy.

While translational motion has no knock on effects to the QPD signal, rotational changes are double counted by both the incident and total field. This results in rotational motion being biased in the QPD signal - even when collecting signals from isotropic scatterers. To prevent this we need to rotate the total field via the inverse rotation matrix of the dimer.

To confirm that our method is producing accurate results, we ran a comparison between our simulative QPD and the results from [4]. Where a 300 nm diameter sphere is scanned across the path of a focused Gaussian beam ($\lambda = 1064$ nm, $NA = 1.2$), the sphere has a refractive index of 1.57 and is suspended in water ($n_{med} = 1.33$) and the condenser lens has its numerical aperture set to 0.5 ($\theta_{max} = 30°$). Scanning across all three primary axis produced the following response curve:

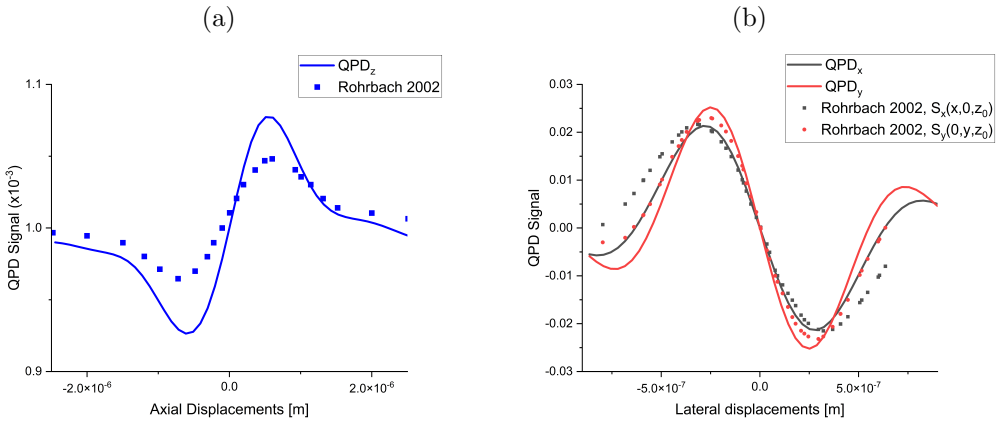

Figure 6.1: Comparison between QPD response signal versus work conducted by Rohrbach, single sphere ($r = 150\ nm$, $n = 1.57$) is scanned by a 1064 nm laser and the QPD signal recorded. Solid lines represent the signal produced by QPD using *ott* and points represent the signal response collected from [4].

The discrepancy between our simulated QPD and the results from Rohrbach can be attributed to the fact that the position to signal error grows as you move further from trap focus. As the particle moves further from the trap focus the error in the attributed signal grows substantially [4]. In most optical trapping experiments we usually are calibrating a strong trap where the mean square displacement falls well within the linear regime shown in fig. 6.1. In which case the error between Rohrbach's model and our own is inconsequential for calibration purposes. With this any trajectory can be collected from the QPD by displacing and rotating the beam accordingly, later in chapters **??** and **??** we discuss the limits of accuracy that can be achieved using back focal plane interferometry to characterise non-spherical targets.

6.2.1 Position detection

In order to accurately capture the dynamics of a trapped particle, a position detection system is required. There are 3 possible methods of position detection: video-analysis, lateral-effect position sensing, and photodiodes.

Video analysis is ideally suited for multiple traps or situations where precision is not the top priority. Whereas lateral-effect and photodiode position detection are two

examples of back-focal plane interferometry, where the interference pattern produced by the target particle is extrapolated to determine its position. In order for video analysis to match the accuracy of back-focal plane interferometry methods requires the camera's frame rate to exceed 1 kHz which can be difficult to achieve while maintaining a decent resolution [3]. In comparison off the shelf back-focal plane detectors can achieve temporal resolutions anywhere from $10 - 100$ kHz [1].

A lateral-effect sensor has a similar output but works using a the entire sensor as a single cell analogous to the focal plane of the trapping beam. The four corners of the sensor act as anodes connected to a base plate cathode, as the beam moves across the surface of the detector each anode will experience a different photocurrent depending on how close the centre of the interference pattern is to each anode. The advantage of a lateral effect detector is that the linear regime is much larger than a QPD making it much better for monitoring the position of a trapped particle. However, Lateral-effect sensors are often limited in their spacial resolution due to high signal-to-noise ratios, requiring a high intensity of light on the sensor in order to get a clean signal. As a result, most optical force measurements are conducted using a QPD as opposed to a lateral-effect sensor, as often the displacement is small enough that the signal-displacement curve can be considered linear.

A quadrant photo diode (QPD) is a frequently used position detection system for optical tweezers due to their high sampling rate, high degree of precision, and ease of set up. The QPD is constructed of four photo diodes assembled in a quadrant formation, when a particle is trapped the interference pattern produced is focused onto the QPD, with the maximum intensity mapping to the particle's centre of mass. By summing the voltages of the horizontal and vertical quadrants together the particle's centre of mass is tracked in the $x - y$ plane. Axial displacement can be estimated by observing the change in the total voltage of the QPD. The outputted signal gives an indication of the particle's relative displacement from the beam focus, but in order to convert the signal to distance units the trap needs to be calibrated (assuming a linear response curve).

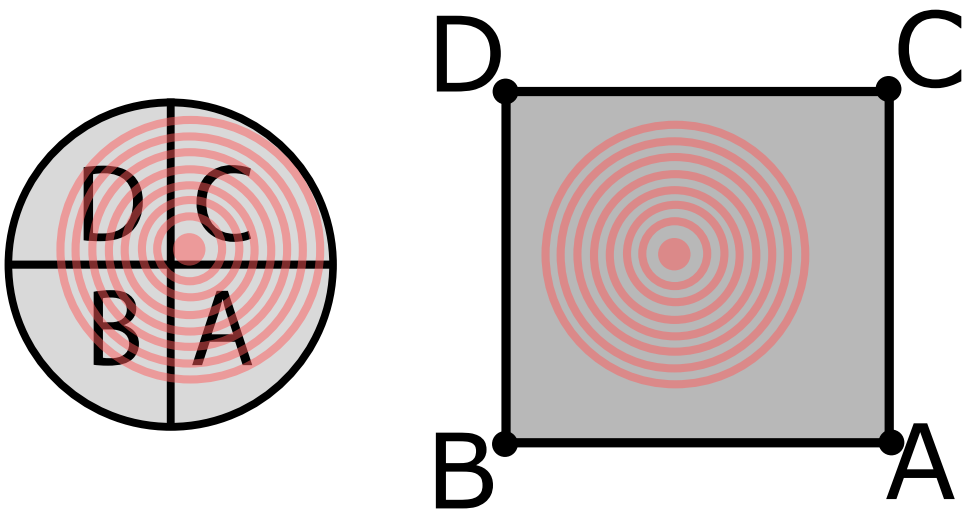

Figure 6.2: Comparison between QPD and Lateral effect photodiodes. The four quadrants of a QPD (left) experience different photocurrents based on the total intensity of light incident on each section (labelled A, B, C, D). Whereas a Lateral effect sensor (right) uses the resistive properties of the photodiode surface to vary the create different photocurrents passing through the anodes A, B, C, and D.

6.3 Characterisation of asymmetric dimer dynamics via PSD analysis

As discussed in **??**, one of the methods developed to work in conjunction with [5] is a simulated quadrant photo diode for as a position detection system. While it is possible to extract all of the relevant dynamics from a simulation, from an experimental standpoint characterising those dynamics is dependent on what experimental techniques are used. Translational motion can be characterised via a position detection system but angular motion is far more difficult to detect, let along characterise.

The simulative QPD is composed of 4 photodiodes that measure the intensity of light incident on their surfaces. Given that the condensing lens will have a maximum

acceptance angle given by its numerical aperture ($\theta_{max} = \sin^{-1}(NA_c/n_{med})$) we define the electric field incident on the QPD surface as the elements of the scattered and incident field that propagate within that angular range of $\pm\theta_{max}$. Using *ott* we can evaluate the total electric field to an arbitrary spacial resolution across the surface of the QPD. The reported signal is found by taking the difference between pairs of quadrant signals (see **??** for further detail). This does not provide a one-to-one result however as hardware errors (i.e. internal resistance, external light sources, and vibrations) would distort the signal. It can be used however to show how if the reported power spectra is an accurate representation of the true particle dynamics or if the additional degrees of freedom have an adverse effect on the scattering. See chapter 2 for a breakdown of power spectral analysis.

As a benchmark we start by considering a single sphere within an optical trap. A single polystyrene sphere suspended in water ($a = 1\mu m$, $n_p = 1.59$, $n_m = 1.33$) was trapped by a focused Gaussian beam ($NA = 1.25$) using circularly polarised light. For the sake of time efficiency the trajectory was sampled every 10 time steps, meaning the upper bound on the power spectra is $f_{Nyq} = f_{sample}/2 = 5000\ Hz$. To optimise the frequency window we fitted the power spectra using the aliased Lorentzian. (Eq. (**??**)).

As shown in fig. 6.3, the two power spectra report different corner frequencies which would be indicate that the trap is not perfectly circular. We can use both *ott* and the trajectory itself to derive an estimation of the trap geometry. Additionally, we fitted the same Lorentzian to the sphere's positional data, this would be a situation when the QPD signals are completely uncorrelated with one another and there is a constant ratio between the QPD signal and the sphere's position. The corner frequencies and corresponding trap stiffness are reported below:

Table 6.1: QPD fitting for single sphere

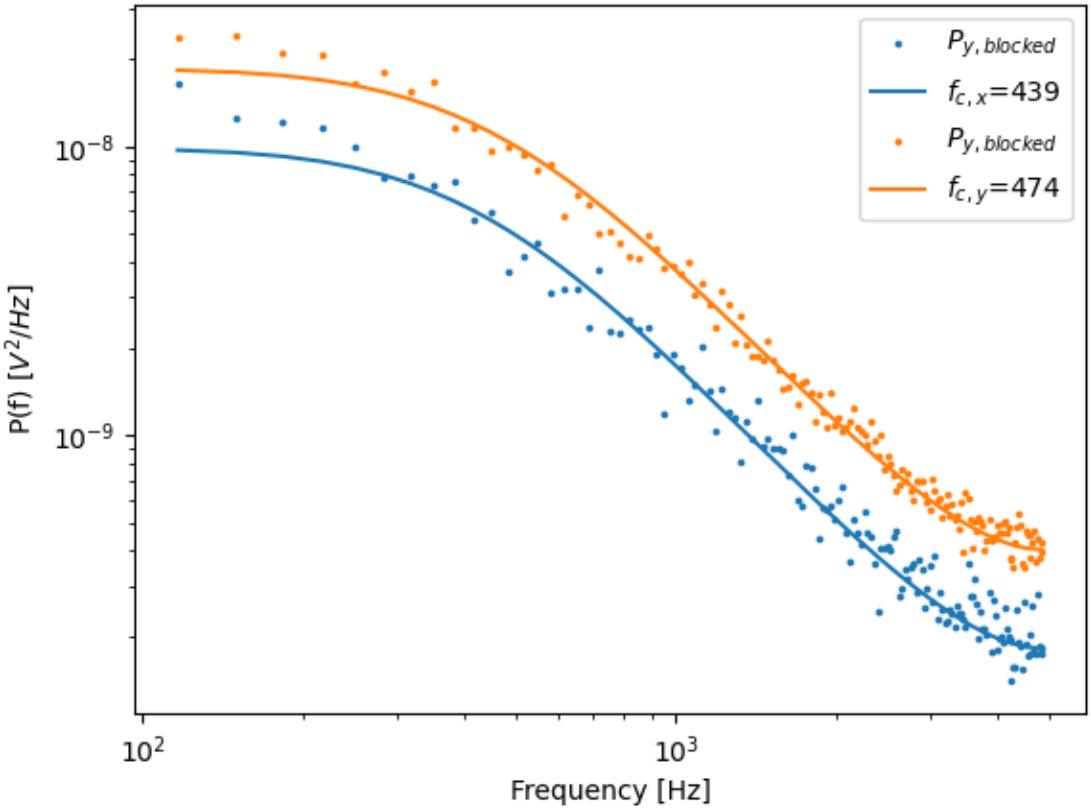

Figure 6.3: Recorded power spectra fitted to eq. **??**, scattered points represents the blocked data ($n_b = 100$). Corner frequency for the Lorentzian curves are reported in the legend.

Fitting parameter	*ott* estimates		QPD fitting		Trajectory fitting	
$f_c\ [Hz]$	447	450	439	474	523	513
$\sigma(f_c)\ [Hz]$	—	—	9.30	9.65	8.67	8.61
$\kappa\ [pN/\mu m]$	53.05	53.40	51.96	56.09	61.94	60.7
Ellipticity	8.16 %		27.17 %		13.8 %	

Where $\sigma(f_c)$ is computed from [1], where the variance is based upon our choice of frequency boundaries ($f_{min} : f_{max} = 100\ Hz : 5000\ Hz$). And the ellipticity of the beam is given by $e = (1 - \kappa_y/\kappa_x)^{0.5}$ and is a measure of the symmetry of the beam wavefront. Its clear from these initial results that the QPD is more sensitive to changes along the y-axis than the x-axis when compared to the direct *ott* calculations. This is somewhat reflected in the trajectory results. Typically, even an industrial Gaussian

beam will produce an elliptical diffraction limit spot when heavily focused; in their tutorial for optimizing the PSD analysis, Berg and Sorensen reported a ellipticity of around 15 % after a total calibration time of 80 seconds [1].

The reason for the discrepancies between all 3 methods is due to what is actually being measured. The *ott* estimates are simply looking at the change in the trapping force as you move along a given axis'. In reality, a particle will be freely diffusing within the trap focus meaning over a short calibration time the QPD is only estimating a weighted average of the trapping strength. If calibrated over an long enough time frame you would expect that the resulting power spectra would exactly mirror the *ott* predictions. There is a clear trade off in terms of accuracy and computation time as shorter calibration runs are computationally more efficient but prone to errors. However, it should be noted that the estimation made by the QPD is still less than the results from [1], though this could be due to a lack of external noise signals.

With this in mind, let us consider a symmetric dimer that is optically trapped by the same Gaussian beam. Not only does the dimer's equilibrium position change but it is subjected to rotational motion due to its unequal moments of inertia. This is reflected in the calibration results using the simulated QPD, where we see a drastically different estimation between the *ott* estimate and the QPD estimate.

Table 6.2: QPD fitting for symmetric dimer

Fitting parameter	*ott* estimate		QPD fitting		Trajectory fitting	
f_c $[Hz]$	445	409	431	424	274	285
$\sigma(f_c)$ $[Hz]$	—	—	9.22	9.16	7.82	7.91
κ $[pN/\mu m]$	52.82	48.54	51.13	50.26	32.45	33.75
Ellipticity	28.5 %		12.7 %		13.8 %	

Now we see that the *ott* predicts a more elliptical trap compared to the QPD model which says the trap is far more symmetrical while trapping a symmetric dimer. A potential reason that *ott* no longer expects a circular trap is because that unlike a sphere, the force displacement curve is not strictly harmonic. If we consider a dimer that is some distance from the beam axis, the sphere closest to the trap focus will experience a slightly greater force compared to the sphere further from the trap. As

such its not accurate to assume that the external force $F(x) = \kappa x$ instead we must consider that it is a function of both the position and orientation simultaneously.

This coupling of the translational and orientational motion has been highlighted previously [5], but there effects have not been demonstrated in the context of an experimental situation. We can see from the difference in trajectory and QPD fittings that while our description of the trap shape is very similar (both methods give similar ellipticity values) but the magnitude of the trap strength are significantly different. This is partially explained by the fact that the QPD is not actually measuring the position of the particle but instead the intensity distribution of the total field incident on the QPD surface. In which case if the dimer is rotated slightly the QPD signal will change even if the dimers centre of diffusion remains stationary.

6.3.1 QPD for angular displacement detection

The next logical step is to consider whether or not a QPD can at all be utilised for detection of rotational motion. This has been shown for nano-particles that exhibit periodic rotational motion using by considering the difference in diagonal quadrants [6]. The only difference between these results is the fact that rotation occurs perpendicular to the particle's long axis, whereas dimers rotate about their long axis. The benefit of detecting rotational motion is that one can begin to build a better understanding about how angular momentum is transferred to a dimer which could be extended to more complex particles. This could give some understanding to the results of Chapter 4.

At just a cursory glance it would appear that there is a clear relationship between the QPD signal and the orientation of the dimer. If we look at the QPD signal produced by a dimer as it is rotated we can see that it is equally sensitive to rotations in either the X-Z or Y-Z plane but there is no change in the signal when rotated by in the X-Y plane.

However if we compare this to fig. **??** we can see that the the signal change is dwarfed by the translational motion. So while their is a clear relationship between the two trying to discern between translational and rotational contributions to the QPD

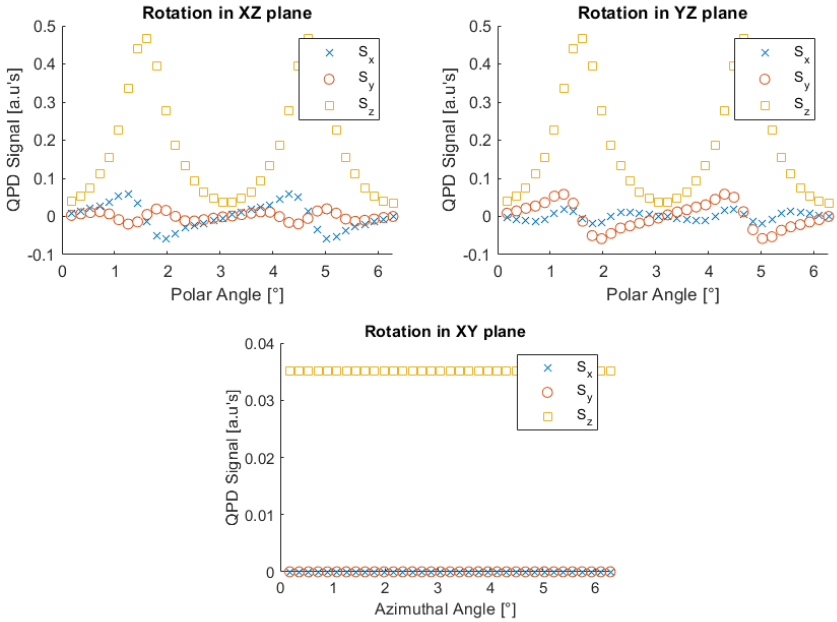

Figure 6.4: QPD signals detected by a dimer being rotated while centred at the focus of the optical trap. Top right: rotation in the X-Z plane. Top left: rotation in the Y-Z plane. Bottom: Rotation in the X-Y plane.

signal is not a simple task. This is significant because it means that with regards to the power spectrum fittings in table 6.2 there is no way of ensuring that the measured trap strengths are accurate. The variance $\sigma(f_c)$ is only the variance based upon our fitting parameters and not on the actual dynamics of the dimer. In the case where the particle's shape is not known prior its not possible to determine whether any inaccuracies in the power spectra are due to the fit or due to the particle's motion.

The dependence of S_x and S_y and the dimer's orientation (defined by the spherical angles θ, ϕ) is therefore not clear. To that end, we utilised machine vector regression, which takes as an input the voltage from the 4 quadrants and tries to fit that to the dimer's trajectory. Fitting the QPD signal to the dimer's position shows promising results, shown in fig 6.4 is a prediction of a symmetric dimer's position based on the QPD signal. With the actual displacement on the x-axis and the predicted result y-axis, and the dashed line represents the y=x line - indicating an ideal prediction.

Fig 6.4 shows that its relatively trivial to predict a particle's position based off the

QPD signal, even in axial direction which has not been done previously. It should be noted that these displacements are relative to the trap focus and so accurate tracking of the beam movements needs to be taken. This result is partially due to the fact that displacement and signal units are linearly related by (**??**). Interestingly when we run the same protocol for different sized dimer's there seems to be a cut off point when the fit begins to fail. Plotting the R^2 for each fit vs its size ratio shows that beyond a size ratio of 5 the machine learning begins to fall off significantly.

This is surprising because we would expect that as the second sphere shrinks the dynamics should more closely approximate that of a single sphere. This should be reflected in the total field incident on the QPD and therefore the machine learning program should be able to easily detect the dimer's translational motion. We can therefore only conclude that the dimer's rotational motion is contributing to the scattering to the scattered field, even if it is miniscule the contribution is enough to throw off a position detection system. Detection of rotational motion was attempted using machine learning, the model was trained on the same trajectory mentioned in **??**, where the dimer is trapped in an off-axis orientation, from a top down perspective it should be easy enough to note that the dimer is not vertically trapped even if the exact angle is difficult to determine.

Overall, the reliance on machine learning to perform vector regression on the collected scattered field is not a viable method for detecting let along characterising the angular displacement of an isotropic scatterer. While there is a clear correlation in the scattered signal and angular displacement the translational motion makes up the majority of the expected signal detected by the QPD. As of now, there is no optical arrangement that would allow rotational motion while restricting translational motion.

Bibliography

[1] Kirstine Berg-Sørensen and Henrik Flyvbjerg. "Power spectrum analysis for optical tweezers". In: 75 (2004), pp. 594–612. ISSN: 0034-6748. DOI: 10.1063/1.1645654.

[2] Lars Friedrich and Alexander Rohrbach. "Tuning the detection sensitivity: a model for axial backfocal plane interferometric tracking". In: *Opt. Lett.* 37.11 (June 2012), pp. 2109–2111. DOI: 10.1364/OL.37.002109. URL: https://opg.optica.org/ol/abstract.cfm?URI=ol-37-11-2109.

[3] Graham M. Gibson, Jonathan Leach, Stephen Keen, et al. "Measuring the accuracy of particle position and force in optical tweezers using high-speed video microscopy". In: *Optics Express* 16.19 (Sept. 2008), p. 14561. ISSN: 1094-4087. DOI: 10.1364/oe.16.014561.

[4] Alexander Rohrbach and Ernst H. K. Stelzer. "Three-dimensional position detection of optically trapped dielectric particles". In: *Journal of Applied Physics* 91.8 (Apr. 2002), pp. 5474–5488. ISSN: 1089-7550. DOI: 10.1063/1.1459748.

[5] Wyatt Vigilante, Oscar Lopez, and Jerome Fung. "Brownian dynamics simulations of sphere clusters in optical tweezers". In: *Optics Express* 28.24 (Nov. 2020), p. 36131. ISSN: 1094-4087. DOI: 10.1364/oe.409078.

[6] Yuval Yifat, John Parker, Tian-Song Deng, et al. "Facile Measurement of the Rotation of a Single Optically Trapped Nanoparticle Using the Diagonal Ratio of a Quadrant Photodiode". In: *ACS Photonics* 8.11 (Nov. 2021), pp. 3162–3172. ISSN: 2330-4022. DOI: 10.1021/acsphotonics.1c00802.